Kovove Mater. 60 2022 247–256
DOI: 10.31577/km.2022.4.247

Precipitation behavior prior to hot roll in the cold-rolled Al-Mg and Al-Mg-Zr alloys

Mohammad Salim Kaiser[1]*, Hossain M. Mamun Al Rashed[2]

[1] *Directorate of Advisory, Extension and Research Services, Bangladesh University of Engineering and Technology, Dhaka-1000, Bangladesh*
[2] *Department of Materials and Metallurgical Engineering, Bangladesh University of Engineering and Technology, Dhaka-1000, Bangladesh*

Received 30 September 2021, received in revised form 25 May 2022, accepted 26 May 2022

Abstract

Precipitation behavior of directly cold-rolled and prior to hot roll Al-5Mg alloy with ternary zirconium has been examined. Hot-rolled and cold-rolled alloy samples are aged simultaneously isochronally and isothermally for different temperatures and times. Hardness, resistivity, impedance value, and DSC study have been considered to comprehend the precipitation behavior of the differently aged alloys. No age-hardening response is observed for all the alloys, but the directly cold-rolled Zr-added alloy resists the soften behavior than that of prior to hot roll alloy. Precipitation kinetics of Al_3Zr in Al-5Mg-0.3Zr alloys is controlled by the diffusion of zirconium in aluminum. Microstructures display that the Al-5Mg alloy becomes almost fully recrystallized after aging at 300 °C for 300 min. But Zr-added alloys do not show this scenario owing to the presence of metastable fine $L1_2$ Al_3Zr precipitates, which are thermally stable at high aging temperatures.

K e y w o r d s: Al-Mg alloys, rolling, resistivity, precipitation, DSC, microstructure

1. Introduction

Aluminum is the predominant metal in Al alloys, and the typical alloying elements are copper, magnesium, manganese, silicon, tin, zinc, etc. Alloys in which magnesium is the principal alloying element, according to the aluminum alloys designation system, are selected 5xxx series alloys [1, 2]. Beryllium, cerium, chromium, gallium, titanium, zirconium, vanadium, etc., may be added to the alloys as minor alloying elements. These Al-Mg alloys have been widely used in boat hulls, dump truck bodies, petrol tanks, cryogenic pressure vessels, packaging, general engineering industries, and other products exposed to marine environments. It is because of their good combination of high strength-to-weight ratio and formability, high ductility, excellent corrosion resistance, and weldability [1, 3]. These series of alloys constitute a group of non-heat-treatable alloys with medium strength. The strength of Al-Mg alloys strongly increases with the addition of Mg as high solubility in solid solutions. These alloys derive their strength mainly from solution strengthening and work hardening during deformation. The fabrication process of 5xxx alloy mainly consists of casting, homogenization, hot rolling, intermediate annealing, and cold rolling [4].

On the other hand, high levels of Mg cause processing challenges and the susceptibility to stress corrosion cracking [5, 6]. An effective alternative method, adding minor alloying elements such as Zr, is used to increase the strength and thermal stability of Al-Mg alloys by forming Al_3Zr dispersoids [7–9]. It is known that cold rolling creates a substructure consisting of a high density of dislocations within grains, cells bounded by arbitrary dislocation boundaries, extended boundaries termed as geometrically necessary boundaries, and shear bands [10, 11]. After high rolling reduction, the formation of a lamellar structure or ultrafine grains may take place, which has a very strong influence on the subsequent anisotropy of

*Corresponding author: tel.: +88-02-9663129; e-mail address: mskaiser@iat.buet.ac.bd

Table 1. Chemical composition of both investigated alloys (wt.%)

Alloy	Mg	Zr	Si	Fe	Sn	Zn	Al
1	5.014	0.000	0.429	0.375	0.249	0.012	Bal.
2	5.124	0.304	0.507	0.269	0.238	0.012	Bal.

the sheet products in high-strength conditions [12]. Numerous studies of microstructural evolution during cold rolling were carried out for aluminum and aluminum alloys [13–15]. At the same time, the structural evolution during extensive rolling and its effect on anisotropy of mechanical properties in high-solute-content Al-Mg alloys containing a dispersion of coherent, nanoscale particles are poorly known. For most non-heat-treatable aluminum alloys, the process usually involves hot rolling, leading to significant thickness reduction and preparation for the later forming process. Rolling is a classic metalworking process that is the standard technique for hardening non-heat-treatable alloys. The rolling operation changes the properties of the surface, like morphological, optical, microstructural, electrochemical, and near-surface regions of the materials, by exercising shear stress on the surfaces.

The present study attempts to understand the precipitation behavior of directly cold-rolled and prior to hot roll Al-5Mg alloys doped with 0.3 wt.% zirconium under thermal treatment. Moreover, Al-5Mg alloy is generally used in a work-hardened condition and will undergo softening during use. But the softening behavior of the alloy system under the influence of hot rolling Al_3Zr particles pre-existing in the matrix has not been studied elaborately. The results are presented along with the analysis of the evolution of microstructures in the experimental alloys due to changes in their chemistry, mechanical, and thermal history.

2. Experimental

In this study, Al-5Mg and Al-5Mg-0.3Zr alloys were prepared through melting of aluminum ingot (99.7 % purity), magnesium lump (99.9 % purity), and Al-10Zr (mass%) master alloys. Melting was done in a resistance heating furnace. The melt temperature was always maintained at 780 ± 15 ℃, and the degasser borax was used as a suitable flux cove. Then the melt was allowed to be homogenized under stirring at 700 ℃ and poured in a preheated at 200 ℃ mild steel mold of 17 × 150 × 250 mm^3. Chemical analysis of both the alloys was performed by Optical Emission Spectrometry. The measured elemental composition by weight percent is presented in Table 1. The cast samples were first machined to skin out the oxide layer from the surface. Size of 20 × 15 × 250 mm^3 for hot and cold rolling and 15 × 15 × 250 mm^3 for direct cold rolling were prepared from the castings. Some samples from both the alloys were kept in a resistance heating furnace at 400 ℃ for 12 h for homogenization. The homogenized samples were solutionized at 530 ℃ for 2 h and then quenched in ice-cooled salt water. At 400 ± 5 ℃ hot rolling of homogenized samples was performed in a lab-scale of 10 HP capacity rolling mill. Then the sample size attained the dimension of 15 × 15 × 250 mm^3 like the cold-rolled sample. As-cast and hot-rolled samples of both the alloys were cold rolled using the same rolling mill up to the reduction of 80 %. The deformation given was about 1.0 mm per pass. Samples of 15 × 15 × 3 mm^3 in size were prepared from the cold-rolled sheet for these studies. Cold-rolled samples were aged isochronally for 60 min at different temperatures up to 500 ℃. The samples were isothermally aged at 200 and 300 ℃ for different times ranging from 15 to 300 min. The hardness of different processed alloys was measured in a Vickers hardness testing machine using a load of 1 kg for 10 s to review the age-hardening effect of the alloys. The electrical conductivity of those processed alloys was carried out with an Electric Conductivity Meter, type 979. Before the experiment, a 15 × 15 mm^2 finished surface was prepared by grinding and polishing. Electric resistivity was calculated from those conductivity data. The directly cold-rolled and prior to hot roll alloys have also been subjected to differential scanning calorimetry using a DuPont 900 instrument under an inert N_2 gas atmosphere. The samples for DSC studies were selected as lumps of 25 mg in weight cleaned with alcohol and acetone before the test. A fixed heating rate of 10 ℃ min^{-1} was used for the DSC scan, and the temperature range was selected from 50 to 600 ℃. The activation energy of transformations in different conditions was calculated using the Nagasaki-Maesono analysis [16]. The optical metallography of the samples was carried out with the help of a Versamet-II-Microscope using conventional metallographic techniques. The specimens were finally polished with alumina and chemically etched with Keller's reagent. The SEM investigation and EDX analysis of the alloys were carried out using a Jeol Scanning Electron Microscope type of JSM-5200 and equipped with an energy dispersive X-ray analyzer.

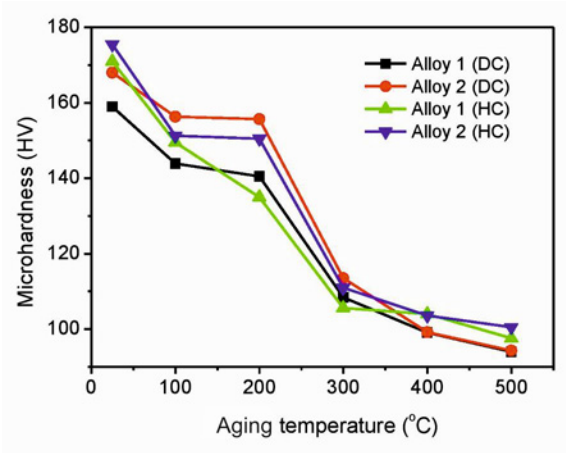

Fig. 1. Variation of microhardness of the cold-rolled Al-Mg Alloy 1 (DC), Al-Mg-Zr Alloy 2 (DC), and prior to hot roll Al-Mg Alloy 1 (HC), Al-Mg-Zr Alloy 2 (HC), isochronally aged for 1 h.

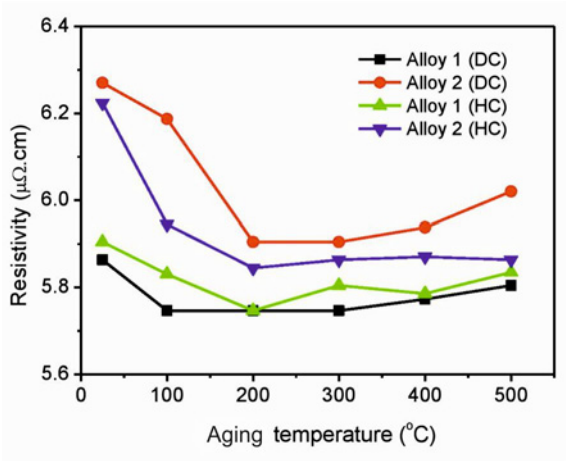

Fig. 2. Variation of resistivity of the experimental alloys isochronally aged for 1 h.

3. Results and discussion

3.1. Aging behavior

3.1.1. Isochronal aging

Isochronal aging curves of the directly cold-rolled Al-Mg Alloy 1 (DC), Al-Mg-Zr Alloy 2 (DC), and prior to hot roll Al-Mg Alloy 1 (HC), Al-Mg-Zr Alloy 2 (HC) aged for 60 min at different temperatures are shown in Fig. 1. It is apparent that there is no age-hardening effect in the alloys. It is recognized that binary Al-Mg alloy is one of the non-age hardenable alloys that form its GP zone at low temperatures [17]. However, during the initial period of aging, considerable softening may occur due to stress relieving as well as the recovery process of the alloys. Alloys containing Zr record higher hardness values in the cold-rolled and followed by prior hot- and cold-rolled conditions. Thus, the cold rolling increases work hardening strength due to the stable dislocation density and sub-grain structure. In the literature, the effect of zirconium addition to aluminum alloys has been well documented. Zirconium produces Al_3Zr particles, which hinder the dislocation slip, keep the intermediate subboundaries stable, and enhance the recrystallization and grain growth resistance. When the alloys are aged at a higher temperature beyond 200 ℃, a sharp decrease in hardness is observed for all the alloys. Because in higher temperatures, the precipitates tend to become coarser and coarse precipitates are not as effective as finely dispersed precipitates in resisting dislocation movement. Coarse precipitates also do not offer enough resistance to the recrystallization as seen for the prior to hot-rolled Al-Mg-Zr Alloy 2 (HC). The softening of the alloys at a higher temperature may be due to particle coarsening as well as the recrystallization effect.

The resistivity curve in Fig. 2 shows that the initial drop in resistivity is recorded in all the experimental alloys. It is because the cold worked alloys during isochronal aging are thought to be due to rearrangement of dislocations. At higher aging temperatures, precipitates coarsening seems to have occurred due to a higher fall of resistivity. For Zr-added alloys, Al-Mg-Zr Alloy 2 (DC) and prior to hot-rolled Al-Mg-Zr Alloy 2 (HC), the resistivity is seen to be higher at an entire aging time. This signifies that the addition of Zr refines the grain structure and leads to the formation of fine Al_3Zr precipitates that increase the resistivity of the alloy.

3.1.2. Isothermal aging

When the alloys are isothermally aged at 200 and 300 ℃, again, no aging response has been observed, but the initial softening is observed for all the alloys (Figs. 3, 4). Directly cold-rolled Al-Mg Alloy 1 (DC) and prior to hot-rolled Al-Mg Alloy 1 (HC) show a very fast and steep decrease in hardness and got behind a constant value. The softening rate is always observed to be low in directly cold-rolled Al-Mg-Zr Alloy 2 (DC), followed by prior to hot-rolled Al-Mg-Zr Alloy 2 (HC). The Zr-added alloys form Al_3Zr precipitates during casting and aging. The dispersedly distributed Al_3Zr particles hinder the dislocation movement, decreasing the softening rate. The Zr added hot-rolled alloy loses to some extent the effectiveness to resist the movement of dislocation due to precipitate coarsening that already took place during homogenizing at 400 ℃ for 12 h, solutionizing at 530 ℃ for 2 h and soaking at hot-rolling temperature, 400 ℃. The decreasing initial hardness of the alloys is due to the recovery process. The magnitude of initial hardness drop is a function

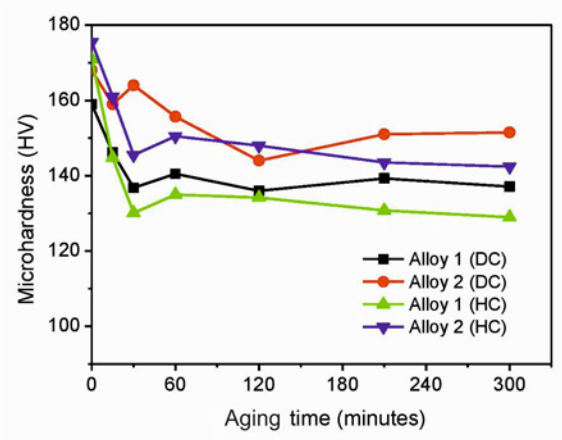

Fig. 3. Isothermal aging curve of the cold-rolled Al-Mg Alloy 1 (DC), Al-Mg-Zr Alloy 2 (DC), and prior to hot roll Al-Mg Alloy 1 (HC), Al-Mg-Zr Alloy 2 (HC), aged at 200 °C.

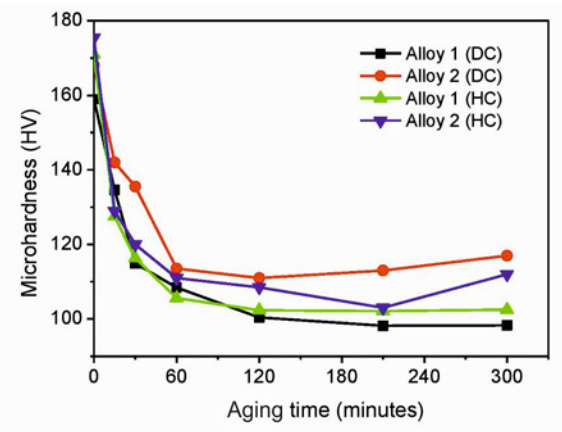

Fig. 4. The isothermal aging curve of the experimental alloys, aged at 300 °C.

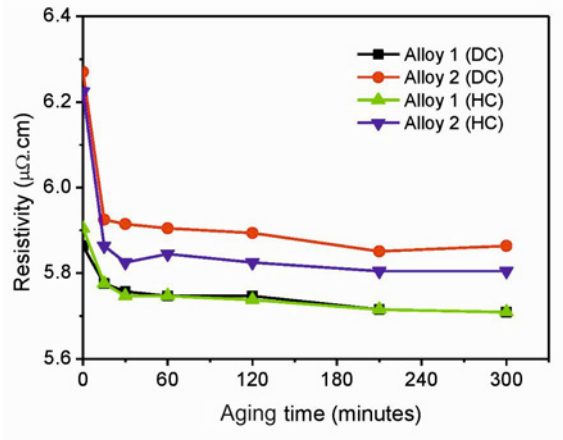

Fig. 5. Variation of resistivity due to isothermal aging of the experimental alloys at 200 °C.

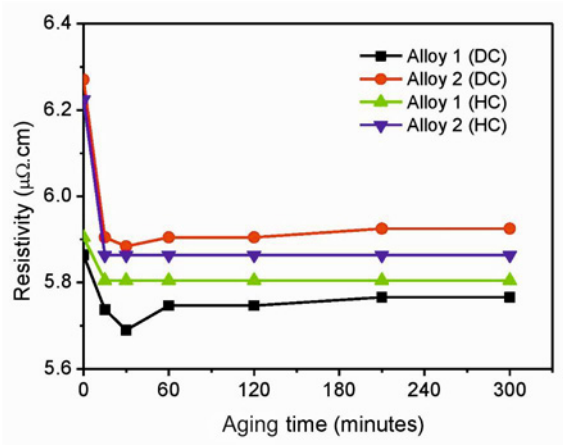

Fig. 6. Variation of resistivity due to isothermal aging of the experimental alloys at 300 °C.

of aging temperature and is found to increase with increasing aging temperature due to higher dislocation mobility.

The isothermal aging curve at 200 °C lower aging temperature showed that the directly cold-rolled alloys attained inferior hardness at the intermediate time around 120 min. It is due to the dissolution of GP zones to the formation of metastable phases while the metastable precipitates have not grown; their size is too small to resist dislocation movement effectively. But this scenario is absent for hot-rolled alloys as it already occurs during hot rolling [18, 19].

The variations of resistivity during isothermal aging of the alloys at 200 and 300 °C are shown in Figs. 5 and 6, respectively. The resistivity curves of the alloys show an initial drop followed by the constant value. The initial drop in resistivity during isothermal aging of the experimental alloys indicates dislocation rearrangement, precipitation coarsening, and recrystallization within the cold-worked alloys. The decrease in resistivity is much higher in binary Al-5Mg alloy than in Zr-added alloy. During aging, Zr-added alloys form the fine precipitates of Al_3Zr, which hamper the reduction of resistivity of the alloys. This phenomenon is more profound for the directly cold-rolled alloys because the hot-rolled alloy loses the effectiveness during socking and rolling at higher temperatures through Al_3Zr precipitates coarsening. For annealing at a higher temperature, the initial drop in resistivity is observed within a short time, as discussed earlier, since higher aging temperatures make higher dislocation mobility of the materials [20].

3.2. Impedance behavior

The frequency dependence of the impedance be-

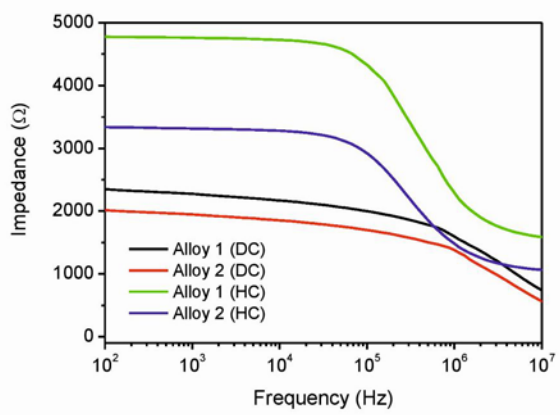

Fig. 7. Impedance behavior of the alloys as a function of the applied frequency.

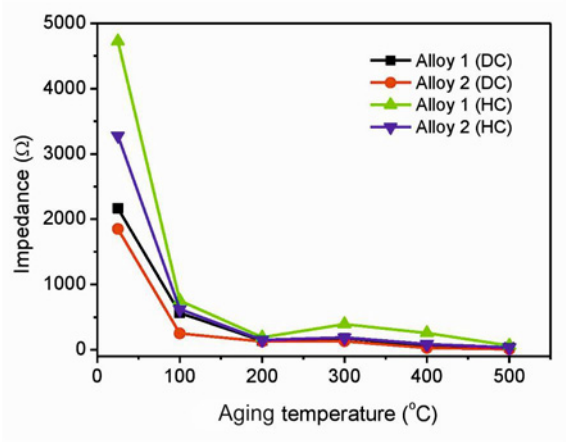

Fig. 8. The behavior of the impedance with the temperature at 10^4 Hz frequency.

havior of the directly cold-rolled Al-Mg Alloy 1 (DC), Al-Mg-Zr Alloy 2 (DC), and prior to hot roll Al--Mg Alloy 1 (HC), Al-Mg-Zr Alloy 2 (HC) at room temperature can be seen in Fig. 7. It has been observed that all of the samples exhibited relatively high impedance at low frequencies, and it decreased with increasing the frequency. In conformity with Drude Lorentz's model, capacitive impacts are elevated at lower frequencies due to the dispersive effect of the electrons colliding with the lattice and electric polarization of the bound electrons, not in the conduction band. Some interfacial polarization effects may also appear. This leads to the high impedance at lower frequencies as it combines both the capacitive and purely resistive effects. Adding Zr significantly decreases the impedance characteristics for both rolling conditions [21]. As fine grains are formed and more grain boundaries of a thin layer are generated, impedance reduces. With the rise of rolling deformation, dislocation density increases, and a serious change of grain orientation causes higher impedance values for hot- and cold--rolled samples. The impedance at 10^4 Hz frequency of the experimental alloys at different aging temperatures for 1 h is shown in Fig. 8. All the alloys exhibit a higher value of impedance while aging is done. The intensity of impedance of all the samples shows a sharp decreasing trend. The dislocation rearrangement has caused a reduction in impedance. The formation of fine-intermetallic precipitation has caused a slight increase in impedance [22].

3.3. Thermal analysis

The directly cold-rolled Al-Mg Alloy 1 (DC), Al--Mg-Zr Alloy 2 (DC), and prior to hot-rolled Al-Mg Alloy 1 (HC), Al-Mg-Zr Alloy 2 (HC) have given rise to the DSC heating curve as shown in Fig. 9. All the DSC heating curves of the experimental alloys are similar in nature, where three peaks are present. The first

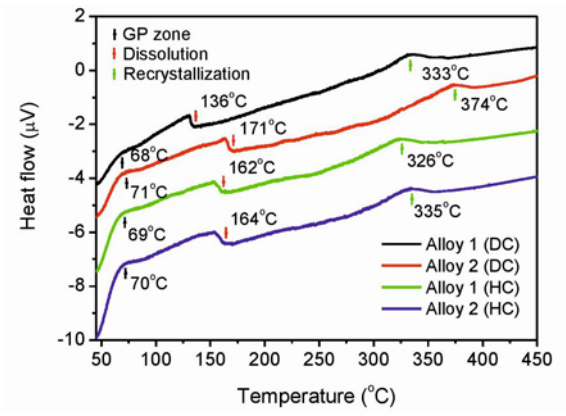

Fig. 9. DSC heating curve of the experimental alloys.

one, an exothermic peak around 70 ℃, is attributed to the formation of GP zones. The activation energy of the process, 60–64 kJ mol^{-1}, is close to the activation energy for GP zone formation, as reported earlier to be 59.9 kJ mol^{-1} [23]. The peak temperatures and corresponding activation energy of the alloys studied are presented in Table 2. A second broad endothermic peak occurs around 136–164 ℃, which refers to the dissolution of some metastable phase as Al-Mg alloy always contents during casting. The activation energy of the process is close to the activation energy for the diffusion of magnesium in aluminum, as an earlier study has been reported to be 130 kJ mol^{-1} [20, 24]. Finally, exothermic peaks around 326–374 ℃ represent recrystallization. However, its activation energy is somewhat higher than the previously reported value of 190 kJ mol^{-1}. This may be due to hindrance to dislocation movement by certain iron aluminides, which might have been present due to the relatively higher iron content in the alloy (~ 0.3 wt.%).

From the respective graph and the table, it is noted

Table 2. Results of DSC heating run

Alloy	Transformation	Peak temperature (°C)	Activation energy (kJ mol^{-1})
Alloy 1 (DC)	GP zone formation	68	62
	Dissolution of some phases	136	135
	Recrystallization	333	202
Alloy 2 (DC)	GP zone formation	71	64
	Dissolution of some phases	171	133
	Recrystallization	374	204
Alloy 1 (HC)	GP zone formation	69	60
	Dissolution of some phases	162	131
	Recrystallization	326	191
Alloy 2 (HC)	GP zone formation	70	61
	Dissolution of some phases	164	129
	Recrystallization	335	192

Remarks:
– Alloy 1 (DC) is a directly cold-rolled Al-Mg alloy,
– Alloy 2 (DC) is a directly cold-rolled Al-Mg-Zr alloy,
– Alloy 1 (HC) is a hot- and cold-rolled Al-Mg alloy,
– Alloy 2 (HC) is a hot- and cold-rolled Al-Mg-Zr alloy.

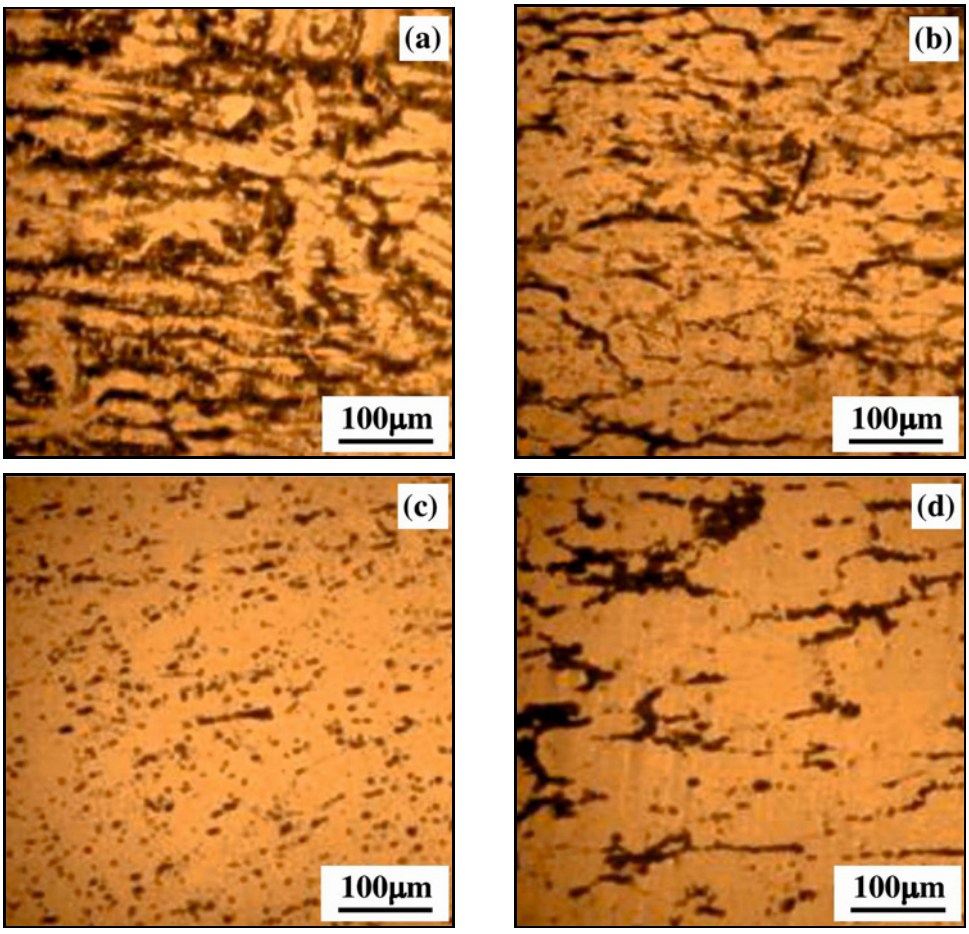

Fig. 10. Optical micrograph of (a) Al-Mg Alloy 1 (DC), (b) Al-Mg-Zr Alloy 2 (DC), (c) Al-Mg Alloy 1 (HC), and (d) Al-Mg-Zr Alloy 2 (HC).

that the Zr added directly cold-rolled Al-Mg-Zr Alloy 2 (DC) always shows all the processes delayed, but this scenario is absent for prior to hot roll Al-Mg-Zr Alloy 2 (HC). In the literature, the effect of zirconium ad-

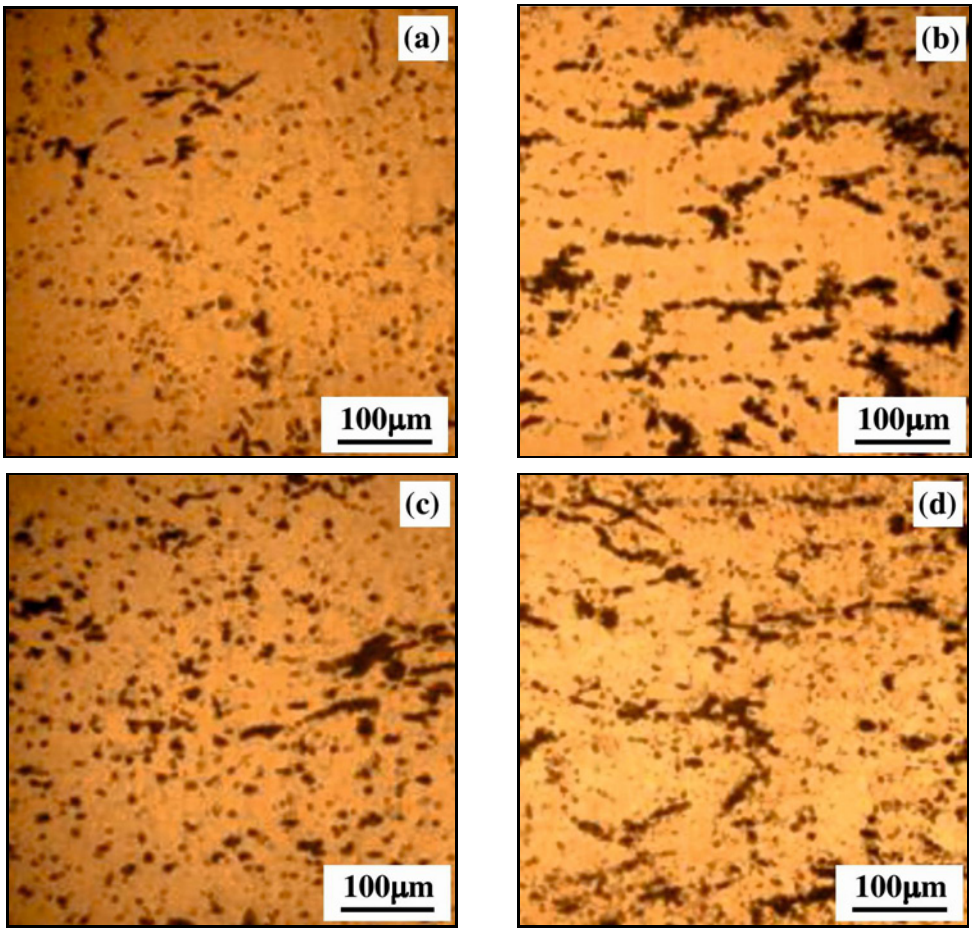

Fig. 11. Optical micrograph of (a) Al-Mg Alloy 1 (DC), (b) Al-Mg-Zr Alloy 2 (DC), (c) Al-Mg Alloy 1 (HC), and (d) Al-Mg-Zr Alloy 2 (HC), aged at 300 °C for 300 min.

dition to aluminum alloys has been well documented. During solidification, it produces Al_3Zr particles that hinder the dislocation slip, keep the intermediate subboundaries stable, and enhance the recrystallization resistance. Based on these reasons, the entire process of thermal stability of the alloy has been delayed. Prior to hot rolling Al-Mg Alloy 1 (HC), Al-Mg-Zr Alloy 2 (HC) does not show the dissolution peak at those temperatures because some existing precipitates are dissolved during heating and soaking for hot working. This thermal process also coarsens the Zr precipitates of the Al-Mg-Zr Alloy 2 (HC). The coarsening Al_3Zr precipitates also reduced the effectiveness of the thermal stability of the alloy [25].

3.4. Optical micrographs

The microstructures of the experimental alloys Al--Mg and Al-Mg-Zr, both the directly cold-rolled and prior to the hot-rolled state, are shown in Fig. 10. Directly cold-rolled Al-Mg Alloy 1 (DC) microstructure displays the as usual α-Al dendrites with coarse grains where the β-Al_8Mg_5 intermetallics along with aluminides of other trace elements stay in the interdendritic regions (Fig. 10a). The directly cold-rolled Al-Mg-Zr alloy 2 (DC) shows the refined primary dendrites α with consequent diminution of dendrite arm spacing (Fig. 10b). This implies the low growth restriction effect. The significant grain refinement of the alloy through the Zr addition can be credited to the heterogeneous nucleation, which is facilitated by the formation of Al_3Zr particles [26, 27]. Due to cold rolling, the alloys exhibit elongated and fragmented dendrites along the rolling direction. In the case of prior to the hot roll, both alloys show signs of the equiaxed grain structures (Figs. 10c,d). During hot rolling at 400 °C, most of the dendritic structure and eutectic phases are dissolved into an equiaxed structure, and the intermetallics are distributed in the interdendritic regions. The cold rolling of the hot-rolled alloys creates typically strained and elongated grains along the rolling direction.

Figure 11 presents the optical microstructures of the above experimental alloys subjected to aging at 300 °C for 300 min. In both rolling conditions, Al-Mg alloy exhibits severe equiaxed grains due to recrystallization (Figs. 11a,c). However, in the Zr-added alloys, elongated grains still dominated as they recrys-

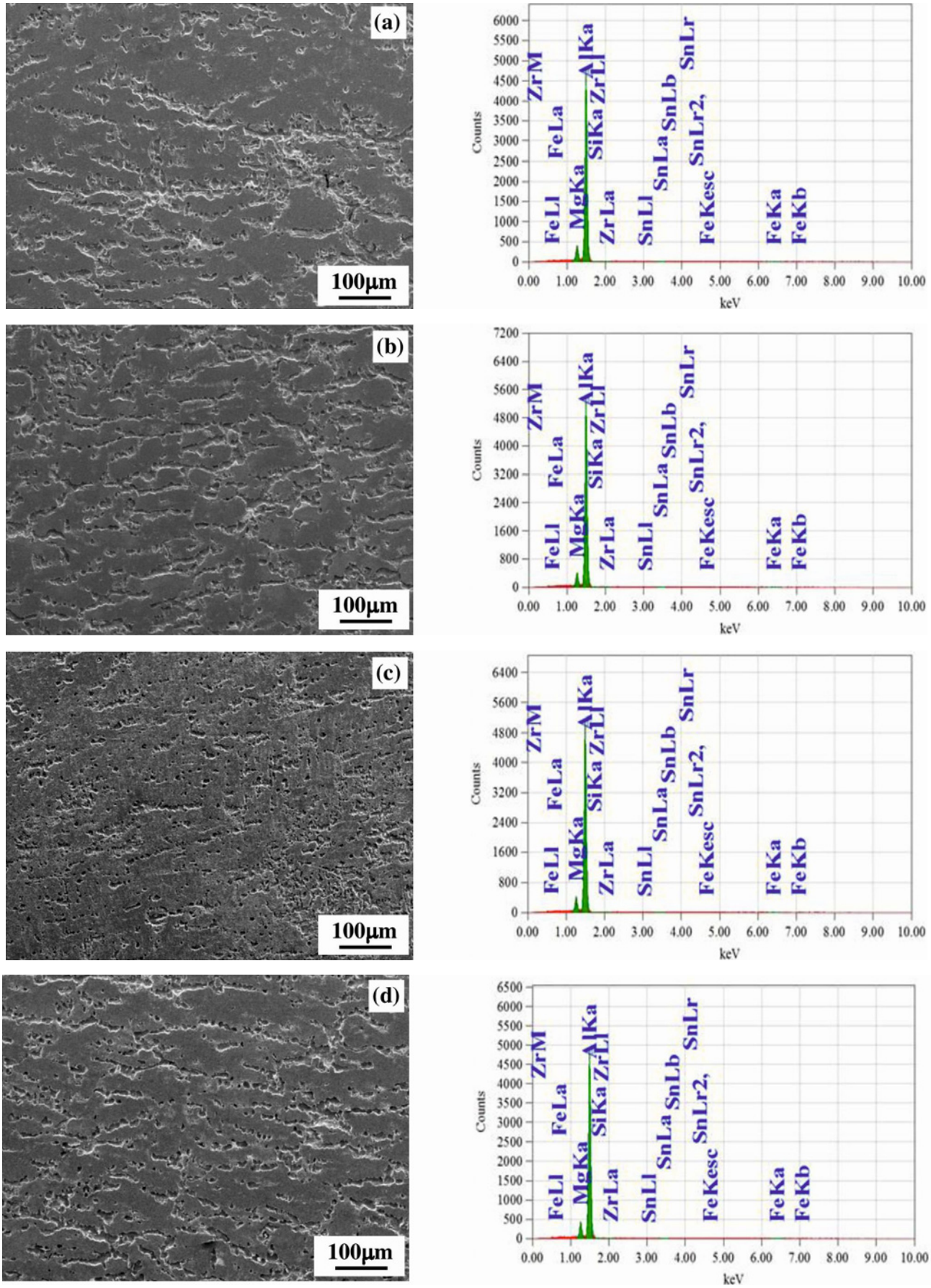

Fig. 12. SEM images and EDX spectra of (a) Al-Mg Alloy 1 (DC), (b) Al-Mg-Zr Alloy 2 (DC), (c) Al-Mg Alloy 1 (HC), and (d) Al-Mg-Zr Alloy 2 (HC), aged at 200 °C for 1 h.

tallized partially (Figs. 11b,d). The recrystallization of Zr-added alloys having fine precipitates of Al_3Zr does not complete at the same temperature. The fine precipitates of Al_3Zr are coherent with the matrix, impeding dislocation slip and effectively pinning subboundary and grain boundary. As a result, aging temperature grain growth and recrystallization are difficult in aluminum alloys [28].

3.5. SEM and EDX observation

Scanning electron microstructures of the experimental alloys aged at 200 ℃ for 1 h that substantiate the observations through optical microstructures are shown in Fig. 12. The directly cold-rolled Al-Mg Alloy 1 (DC) and Al-Mg-Zr Alloy 2 (DC) show the elongated grain, but Zr-added alloy consists of relatively refined grains in the microstructure (Figs. 12a,b). It has already been stated earlier about the refining properties of Zr. There is no evidence of recrystallization, and it keeps hold of its elongated grains after aging at 200 ℃ for 1 h. Fracture surfaces are observed along with the grain boundary. The increasing magnesium content in the alloy can increase the work hardening rate. Alloys containing more than 3 wt.% Mg undergo sensitization, wherein the magnesium segregates from the solid solution, and this leads to a higher tendency for intercrystalline failure, presumably due to the formation of β-phase Al_8Mg_5 or Al_3Mg_2 precipitates at the slip band and grain boundaries. Upon cold working, this particular problem is aggravated [29, 30]. As a result, fracture surfaces remain in the grain boundary. It is also demonstrated that the Zr bearing alloys show a relatively thin grain boundary fracture because of relatively fine grains. The corresponding EDX analysis by weight percent of the SEM confirms that Al-Mg Alloy 1 (DC) consists of a weight amount of 93.45 % Al, 5.65 % Mg, 0.11 % Si, 0.52 % Fe, and 0.27 % Sn. Similarly Al-Mg-Zr Alloy 2 (DC) contains 93.44 % Al, 5.10 % Mg, 0.04 % Si, 0.98 % Fe, 0.18 % Sn, and 0.25 % Zr.

Scanning electron microstructures of prior to hot-rolled Al-Mg Alloy 1 (HC) aged at similar conditions show partially recrystallized grains with ample second phase particles at the grain boundaries (Fig. 12c). Heavily rolled both hot- and cold-rolled samples started the process of recrystallization earlier. However, no evidence of recrystallization of Al-Mg-Zr Alloy 2 (HC) (Fig. 12d) is viewed. The corresponding EDX analysis by weight percent of the SEM corroborates that Al-Mg Alloy 1 (DC) consists of a weight amount of 93.27 % Al, 5.45 % Mg, 0.13 % Si, 0.97 % Fe, 0.12 % Sn, and 0.06 % Zr. Similarly Alloy 2 contents 93.22 % Al, 5.37 % Mg, 0.13 % Si, 0.95 % Fe, 0.03 % Sn, and 0.30 % Zr.

4. Conclusions

It is evident that no age-hardening effect is observed due to the addition of Zr in the Al-5Mg alloy. However, during aging, relatively lower softening is noticed than in the base alloy since Zr produces Al_3Zr particles during solidification, and aging hinders the dislocation movement into the cold-rolled alloys. As a result, the whole thermal processes of the alloys are delayed, like GP zone formation, dissolution of some phases, and recrystallization. The dendrites nature of the Al-Mg alloy microstructure is refined substantially with the addition of zirconium through the heterogeneous nucleation of Al_3Zr particles. The hot-rolled alloys after aging show minimum positive response due to prior precipitation coarsening of Al_3Zr in zirconium-bearing alloys during homogenizing and soaking at the hot-rolling temperature, and these precipitates are not as effective as finely dispersed precipitates in resisting the movement of dislocation.

Acknowledgements

The authors are very grateful to the Directorate of Advisory, Extension and Research Services of Bangladesh University of Engineering & Technology, Dhaka-1000, for all the support. The authors also acknowledge the facilities of the Department of Glass and Ceramics.

References

[1] I. Polmear, Light Alloys, 4th ed., Butterworth-Heinemann, 2005, ISBN: 9780080496108.

[2] M. S. Kaiser, Fractional recrystallization behaviour of Al-Mg alloy with different Sc addition content, International Journal of Materials Science and Engineering 2 (2014) 136–140. https://doi.org/10.12720/ijmse.2.2.136-140

[3] X. Li, W. Xia, H. Yan, J. Chen, X. Li, Improving strength and corrosion resistance of high Mg alloyed Al-Mg-Mn alloys through Ce addition, Corrosion Engineering Science and Technology 55 (2020) 381–391. https://doi.org/10.1080/1478422X.2020.1735716

[4] B. Wang, X. H. Chen, F. S. Pan, J. J. Mao, Y. Fang, Effects of cold rolling and heat treatment on microstructure and mechanical properties of AA 5052 aluminum alloy, Transactions of Nonferrous Metals Society of China 25 (2015) 2481–2489. https://doi.org/10.1016/S1003-6326(15)63866-3

[5] Z. Zhu, X. Jiang, G. Wei, X. Fang, Z. Zhong, K. Song, J. Han, Z. Jiang, Influence of Zn content on microstructures: Mechanical properties and stress corrosion behavior of AA5083 aluminum alloy, Acta Metallurgica Sinica (English Letters) 33 (2020) 1369–1378. https://doi.org/10.1007/s40195-020-01063-7

[6] M. O. Speidel, M. V. Hyatt, Stress-Corrosion Cracking of High-Strength Aluminum Alloys. In: Fontana, M. G., Staehle, R. W. (Eds.), Advances in Corrosion

Science and Technology, vol. 2. Springer, Boston, 1972. https://doi.org/10.1007/978-1-4615-8255-7_3
[7] Z. Yin, Q. Pan, Y. Zhang, F. Jiang, Effect of minor Sc and Zr on the microstructure and mechanical properties of Al-Mg based alloys, Materials Science and Engineering A 280 (2000) 151–155. https://doi.org/10.1016/S0921-5093(99)00682-6
[8] M. Schuster, A. D. Luca, A. Mathur, E. Hosseini, C. Leinenbach, Precipitation in a 2xxx series Al-Cu-Mg-Zr alloy fabricated by laser powder bed fusion, Materials & Design 211 (2021) 110131. https://doi.org/10.1016/j.matdes.2021.110131
[9] J. R. Croteau, J. G. Jung, S. A. Whalen, J. Darsell, A. Mello, D. Holstine, K. Lay, M. Hansen, D. C. Dunand, N. Q. Vo, Ultrafine-grained Al-Mg-Zr alloy processed by shear-assisted extrusion with high thermal stability, Scripta Materialia 186 (2020) 326–330. https://doi.org/10.1016/j.scriptamat.2020.05.051
[10] M. S. Kaiser, Properties of Al-6Mg-xSc (x = 0 to 0.6 wt.%) alloy subjected to thermal treatment: A Review, Reviews on Advanced Materials and Technologies 3 (2021) 42–54. https://doi.org/10.17586/2687-0568-2021-3-1-42-54
[11] C. Hong, X. Huang, G. Winther, Dislocation content of geometrically necessary boundaries aligned with slip planes in rolled aluminium, Philosophical Magazine A 93 (2013) 3118–3141. https://doi.org/10.1080/14786435.2013.805270
[12] V. A. Kulitskiy, S. S. Malopheyev, R. Kaibyshev, Effect of cold rolling on microstructure and mechanical properties of an Al-Mg-Sc-Zr alloy, Advanced Materials Research 922 (2014) 388–393. https://doi.org/10.4028/www.scientific.net/AMR.922.388
[13] W. Wen, Y. Zhao, J. G. Morris, The effect of Mg precipitation on the mechanical properties of 5xxx aluminum alloys, Materials Science and Engineering A 392 (2005) 136–144. https://doi.org/10.1016/j.msea.2004.09.059
[14] C. Q. Huang, J. P. Diao, H. Deng, B. J. Li, X. H. Hu, Microstructure evolution of 6016 aluminum alloy during compression at elevated temperatures by hot rolling emulation, Transactions of Nonferrous Metals Society of China 23 (2013) 1576–1582. https://doi.org/10.1016/S1003-6326(13)62633-3
[15] G. F. Dirras, M. P. Biget, C. Rey, On the microstructural evolution of cold-rolled Al + 5 at.% Mg, Scripta Metallurgica et Materialia 33 (1995) 755–760. https://doi.org/10.1016/0956-716X(95)00288-7
[16] S. Nagasaki, A. Maesono, High Temperatures – High Pressures (HTHP), Metals Physics 11 (1965) 182–188.
[17] M. Howeyze, A. R. Eivani, H. Arabi, H. R. Jafarian, N. Park, The effect of amount of pre-strain using equal channel angular pressing on softening response of AA5052 alloy, Journal of Materials Research and Technology 9 (2020) 6682–6695. https://doi.org/10.1016/j.jmrt.2020.04.065
[18] M. S. Kaiser, Effect of solution treatment on the age hardening behaviour of Al-12Si-1Mg-1Cu piston alloy with trace Zr addition, Journal of Casting and Materials Engineering 2 (2018) 30–37. https://doi.org/10.7494/jcme.2018.2.2.30
[19] A. Elasheri, E. M. Elgallad, N. Parson, X. G. Chen, Evolution of Zr-bearing dispersoids during homogenization and their effects on hot deformation and recrystallization resistance in Al-0.8%Mg-1.0%Si alloy, Journal of Materials Engineering and Performance 30 (2021) 17–28. https://doi.org/10.1007/s11665-021-05917-8
[20] M. S. Kaiser, S. Datta, A. Roychowdhury, M. K. Banerjee, Age hardening behaviour of wrought Al-Mg-Sc alloy, Journal of Materials and Manufacturing Processes 23 (2008) 74–81. https://doi.org/10.1080/10426910701524600
[21] G. R. Olhoeft, Low-frequency electrical properties, Geophysics 50 (1985) 2492–2503. https://dx.doi.org/10.1190/1.1441880
[22] H. M. N. Ahmad, S. Ghosh, G. Dutta, A. G. Maddaus, J. G. Tsavalas, S. Hollen, E. Song, Effects of impurities on the electrochemical characterization of liquid-phase exfoliated niobium diselenide nanosheets, Journal of Physical Chemistry C 123 (2019) 8671–8680. https://doi.org/10.1021/acs.jpcc.9b00485
[23] N. Afify, A. F. Gaber, G. Abbady, Fine scale precipitates in Al-Mg-Zn alloys after various aging temperatures, Materials Sciences and Applications 2 (2011) 427–434. https://doi.org/10.4236/msa.2011.25056
[24] M. J. Starink, A. M. Zahra, Low-temperature decomposition of Al-Mg alloys: Guinier-Preston zones and $L1_2$ ordered precipitates, Philosophical Magazine A 76 (1997) 701–714. https://doi.org/10.1080/01418619708214031
[25] M. S. Kaiser, Solution treatment effect on tensile, impact and fracture behaviour of trace Zr added Al-12Si-1Mg-1Cu piston alloy, Journal of the Institution of Engineers D 99 (2018) 109–114. https://doi.org/10.1007/s40033-017-0140-5
[26] F. Schmid, I. Weibensteiner, M. A. Tunes, T. Kremmer, T. Ebner, R. Morak, P. J. Uggowitzer, S. Pogatscher, Synergistic alloy design concept for new high-strength Al-Mg-Si thick plate alloys, Materialia 15 (2021) 100997. https://doi.org/10.1016/j.mtla.2020.100997
[27] E. Cerri, P. Leo, Influence of severe plastic deformation on aging of Al-Mg-Si alloys, Materials Science and Engineering A 410–411 (2005) 226–229. https://doi.org/10.1016/j.msea.2005.08.135
[28] I. J. Polmear, Role of trace elements in aged aluminium alloys, Materials Science Forum 13/14 (1987) 195–214. https://doi.org/10.4028/www.scientific.net/MSF.13-14.195
[29] M. S. Kaiser, Precipitation and softening behaviour of cast, cold rolled and hot rolling prior to cold rolled Al-6Mg alloy annealed at high temperature, Journal of Mechanical Engineering 45 (2015) 32–36. https://doi.org/10.3329/jme.v45i1.24381
[30] J. Yan, N. M. Heckman, L. Velasco, A. M. Hodge, Improve sensitization and corrosion resistance of an Al-Mg alloy by optimization of grain boundaries, Scientific Reports 6 (2016) 26870. https://doi.org/10.1038/srep26870